Functional Nucleic Acids

International Edition: DOI: 10.1002/anie.201916707
German Edition: DOI: 10.1002/ange.201916707

Supramolecular Fluorescence Resonance Energy Transfer in Nucleobase-Modified Fluorogenic RNA Aptamers

*Christian Steinmetzger, Carmen Bäuerlein, and Claudia Höbartner**

Abstract: *RNA aptamers form compact tertiary structures and bind their ligands in specific binding sites. Fluorescence-based strategies reveal information on structure and dynamics of RNA aptamers. Herein, we report the incorporation of the universal emissive nucleobase analog 4-cyanoindole into the fluorogenic RNA aptamer Chili, and its application as a donor for supramolecular FRET to the bound ligands DMHBI$^+$ or DMHBO$^+$. The photophysical properties of the new nucleobase–ligand-FRET pair revealed structural restraints for the overall RNA aptamer organization and identified nucleotide positions suitable for FRET-based readout of ligand binding. This strategy is generally suitable for binding-site mapping and may also be applied for responsive aptamer devices.*

The unrivaled sensitivity and richness of fluorescence-based techniques allows unique studies of both small molecules and structured biomacromolecules. Fluorogenic aptamers gained increasing interest as functional RNAs that light up conditionally fluorescent small molecules only when these are bound to the RNA.[1] Recent developments include the families of Spinach,[2] Broccoli,[3] Corn[4] and Chili[5] aptamers for hydroxybenzylidene imidazolone (HBI)-derived ligands, Mango[6] variants for thiazole orange as well as the silicon rhodamine-binding SiRA.[7] Such in vitro-selected RNA aptamers have found applications as genetically encodable tags for RNA imaging,[8] as components of biosensors for metabolite detection,[9] and as building blocks for responsive nucleic acid architectures.[10] The apta-FRET concept is based on assembling two fluorogenic aptamers, Spinach and Mango, on an RNA origami framework,[11] enabling energy transfer from DFHBI-1T bound to Spinach, to YO3-biotin complexed by Mango. The knowledge about the structure of the aptamers not only facilitates the optimization of photophysical properties[12] but is also essential for the design of functional devices that depend on the relative orientation of aptamers and their bound ligands.[11]

[*] C. Steinmetzger, C. Bäuerlein, Prof. Dr. C. Höbartner
Institute of Organic Chemistry, University of Würzburg
Am Hubland, 97074 Würzburg (Germany)
E-mail: claudia.hoebartner@uni-wuerzburg.de
Supporting information and the ORCID identification number(s) for the author(s) of this article can be found under: https://doi.org/10.1002/anie.201916707.

In the absence of tertiary structure information of functional RNAs, fluorescence-based methods have contributed immensely to studying RNA structure and folding.[13] Examples include the 2APfold approach,[14] which employs the fluorescent nucleobase analog 2-aminopurine (2AP) and harnesses context- and structure-dependent changes of the fluorescence quantum yields to report on RNA folding and folding kinetics, as impressively demonstrated for various metabolite-binding riboswitches.[15] In the past decades, a number of fluorescent nucleobase analogs (FBAs) have been reported and applied for studies of RNA structure and folding,[16] including isomorphic and isofunctional heterocycles in an emissive RNA alphabet.[17] FRET pairs of FBAs have attracted increasing interest because the readout is not limited to a single position.[18] The rigid placement of isomorphic FBAs inside double-stranded DNA/RNA resulted in FRET efficiencies close to theoretically predicted values[19] and enabled their use as molecular rulers.[20] Another FRET-based strategy using FBAs was developed to screen drug candidates addressing the bacterial ribosome. Fluorescently tagged aminoglycoside antibiotics exhibited donor-sensitized fluorescence emission when binding to a ribosomal A-site construct modified with an emissive uridine analogue.[21]

Unifying these concepts, we introduce a new fluorescent nucleobase analogue–ligand FRET pair for studying RNA aptamer structure and folding. In particular, we investigated the Chili RNA aptamer, which exhibits large Stokes shift fluorescence emission of the cationic HBI chromophores DMHBI$^+$ and DMHBO$^+$ (Figure 1a,b).[5,22] Herein, we demonstrate that these ligands serve as supramolecular FRET acceptors of site-specifically modified RNA aptamers that carry the fluorescent nucleobase analog 4-cyanoindole (4CI) (Figure 1c). We have established the synthesis of 4CI-labeled RNA and characterized the photophysical properties of the environment-sensitive emissive ribonucleoside. Detailed studies of eight Chili aptamer constructs that carried 4CI at different positions enabled the characterization of the free RNA aptamer and its complexes with DMHBI$^+$ and DMHBO$^+$.

4-Cyanoindole was recently introduced as a new universal nucleobase analog for DNA with an emission maximum of 412 nm.[23] Here, we synthesized the corresponding 4CI ribonucleoside (**r4CI**) for RNA solid-phase synthesis starting from 4-cyanoindole and Hoffer's chlorosugar. The detour via the reported 2′-deoxynucleoside (**d4CI**, Figure 2a) was necessary because direct ribosylation reactions, such as the Vorbrüggen reaction with 2,3,5-tribenzoyl-1-acetylribose or nucleophilic substitution of α-haloribose derivatives, were unsuccessful. Similar difficulties have been reported earlier

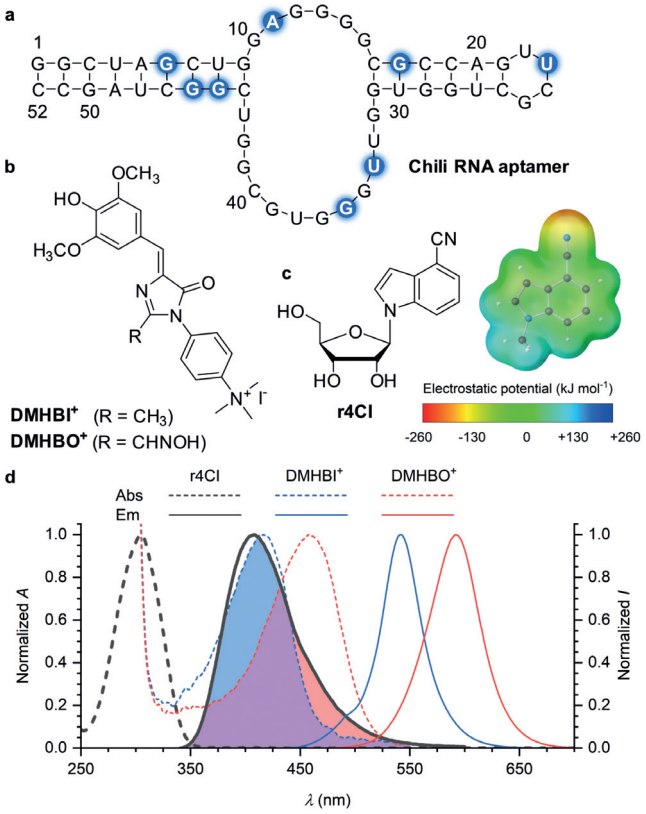

Figure 1. a) Chili RNA aptamer sequence with **r4CI** modification sites indicated in blue. b) Structures of the two fluorogenic ligands (**DMHBI**$^+$, **DMHBO**$^+$) c) Structure and electrostatic potential of the fluorescent 4-cyanoindole ribonucleoside (**r4CI**). d) Absorption and fluorescence emission spectra for the FRET pairs formed between the donor **r4CI** (black) and the acceptor Chili–DMHBI$^+$ (blue) or Chili–DMHBO$^+$ (red). The shaded area indicates spectral overlap between donor emission and acceptor absorption.

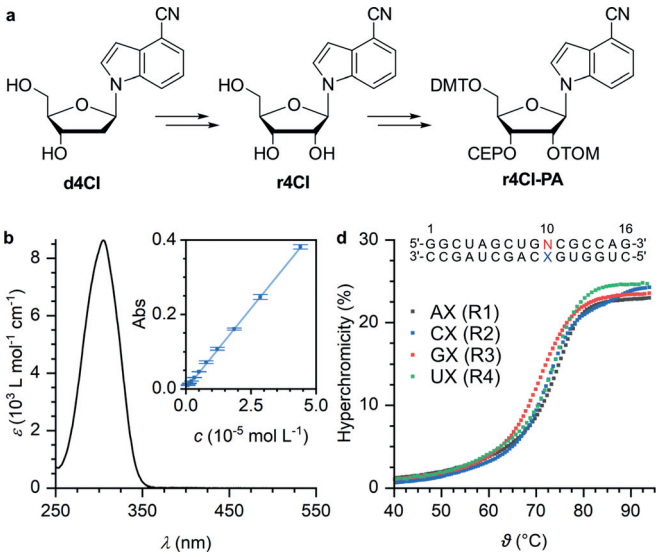

Figure 2. a) Synthetic pathway for **r4CI** phosphoramidite. Details in the Supporting Information. b) UV/Vis spectrum of **r4CI** (PBS, pH 7.4). The extinction coefficient was determined from a linear fit of the absorbance at 305 nm vs. concentration (inset). c) UV melting curves of four 16mer RNA duplexes corresponding to the stem regions of Chili with X = **r4CI** (N = A, C, G, U), 10 μM in PBS, pH 7.4.

for ribosylation of indole derivatives.[24] The 2′-deoxynucleoside **d4CI** was converted into the ribonucleoside **r4CI** through a diastereospecific elimination-dihydroxylation approach (Figure 2a, Scheme S1).[24] The **r4CI** nucleoside was then converted to the corresponding 5′-*O*-DMT-2′-*O*-TOM-protected 3′-*O*-β-cyanoethyl phosphoramidite building block (Scheme S2) and used for solid-phase synthesis.

To study the properties of **r4CI** in the RNA environment, 16nt RNA oligonucleotides were synthesized and hybridized with complementary strands to prepare four duplexes with **r4CI** opposite each of the four standard nucleobases (Figure 2 and the Supporting Information, Tables S1 and S2). Melting temperatures (T_m) and thermodynamic parameters ($\Delta H°$, $\Delta S°$, $\Delta G°_{298K}$) of the duplexes were determined from changes of the absorbance at 260 nm using a non-linear fitting routine (Table S3).[25] The absence of prominent hydrogen-bonding sites and the overall low polarity of 4CI (Figure 1c and Figure S1) allow the accommodation in the duplex opposite any of the natural bases, with T_m values of 69.4, 71.8, 73.2, and 74.3 °C for **r4CI** opposite G, C, U, and A, respectively. Compared to the unmodified base pairs (Figure S2), the formation of 4CI-modified duplexes carries a lower entropic penalty (Table S3), suggesting increased conformational freedom around the modification site.

r4CI has a near-UV absorption maximum at 305 nm with an extinction coefficient of 8640 L mol^{-1} cm^{-1}, and a fluorescence emission maximum at 412 nm with an absolute quantum yield of 0.67 (Figure S3). The excitation maximum of the free nucleoside closely matches that in single- and double-stranded RNA, whereas the emission maximum shows a minor blue shift of 3–5 nm (Table 1). In the single-stranded RNA (ssR4), the fluorescence emission of **r4CI** is reduced by a factor of four (Figure 3a). Reduced quantum yields of FBAs upon incorporation into oligonucleotides is not uncommon and has been observed for many examples, including 2AP[26] and d4CI.[23] In ssR4, the presence of a guanine as the 3′-neighbor of **r4CI** is also partially responsible for the reduced emission because guanine is capable of quenching adjacent fluorophores by photoinduced electron transfer (PET).[27] Stern–Volmer titration of **r4CI** with nucleoside monophosphates shows quenching in the order G ≫ C ≈ U > A (Figure S4a,b) in agreement with the results of a frontier molecular orbital analysis (Figure S4c). Further quenching is observed in the double-stranded RNA (dsR4), likely because an additional guanine is present in the complementary strand forming the 5′-neighboring base-pair of the modification site. The fluorescence decay of **r4CI** in

Table 1: Spectroscopic data for **r4CI**, ssRNA and dsRNA R4 (PBS, pH 7.4).

	$\lambda_{abs,max}$ [nm]	ε_{max} [L mol^{-1} cm^{-1}]	$\lambda_{ex,max}$ [nm]	$\lambda_{em,max}$ [nm]	ϕ	τ[c] [ns]
r4CI	305	8640	303	412	0.67[a]	9.48[d]
ssR4	–	–	303	409	0.17[b]	7.24[e]
dsR4	–	–	304	407	0.05[b]	1.12[e]

[a] Absolute quantum yield. [b] Relative to the fluorescence intensity of r4CI. [c] λ_{ex} = 318 nm, λ_{em} = 410 nm. [d] Monoexponential fit. [e] Amplitude average for triexponential fit.

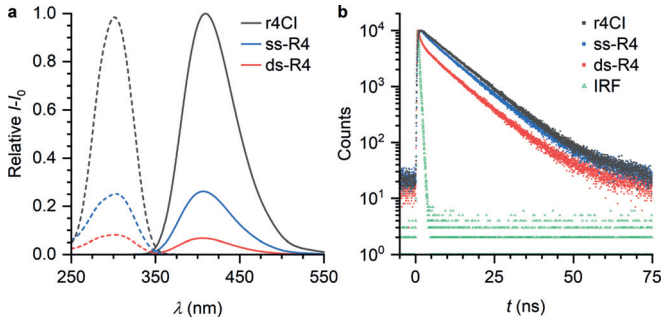

Figure 3. Incorporation of 4CI into oligoribonucleotides leads to partial quenching as shown by a) relative steady-state fluorescence excitation and emission spectra and b) time-resolved fluorescence emission profiles of **r4CI**, ssR4 and dsR4 (1.0 μM, PBS, pH 7.4).

PBS is monoexponential with a lifetime of 9.5 ns (Figure 3b, Table 1). In both ssR4 and dsR4, the decay becomes multi-exponential with a long lifetime component that is similar to free **r4CI** and likely represents an unstacked subpopulation of the fluorophore; two shorter components arise from different degrees of stacking with neighboring bases, which results in fluorescence quenching (Figure S5). Similar decay kinetics have been observed for 2AP in ssDNA and dsDNA.[26] The amplitude average lifetime of **r4CI** in ssR4 is unusually long in relation to the steady-state emission, which indicates formation of a dark state. Similar phenomena have also been observed for other FBAs.[20a]

The emission of **r4CI** strongly overlaps with the absorption bands of conditionally fluorescent HBI derivatives such as $DMHBI^+$ and $DMHBO^+$, which bind to the 52 nt RNA aptamer Chili with nanomolar affinity and consequently become highly emissive (Figure 1d and Figure S6). An **r4CI**-modified Chili–HBI complex therefore constitutes an intra-supramolecular FRET pair, whose Förster radius (R_0) depends on the context-sensitive donor quantum yield in addition to the relative orientation of the FRET partners, which must be considered as static and non-isotropic. We selected eight suitable incorporation sites for **r4CI** within the top and bottom stems, the tetraloop and the internal loop of the aptamer, based on previously reported Tb^{3+} probing and mutagenesis experiments.[5,22] The full-length **r4CI**-labeled Chili aptamers were prepared from two synthetic 26 nt fragments by enzymatic ligation with T4 RNA ligase and characterized by ESI-MS (Tables S1 and S2).

All constructs were intrinsically fluorescent to varying degrees in the absence of ligand with emission maxima ranging from 393 to 404 nm ($\lambda_{ex}=303$ nm, Figure 4a and Figure S7). The respective fluorescence decays were modelled as a sum of two to four exponential terms (Figure S8). The highest fluorescence intensity and least complex decay were observed when **r4CI** replaced U23, the second nucleotide in the UUCG tetraloop. UNCG tetraloops are extraordinarily stable and present a highly conserved structure motif, in which the second nucleotide (N) is flexible and exposed to the solvent (Figure S9). Therefore, **r4CI** at position 23 is subject to fewer quenching interactions than at an intrahelical position, which is reflected by an average lifetime of 6.9 ns and by the highest quantum yield of all eight

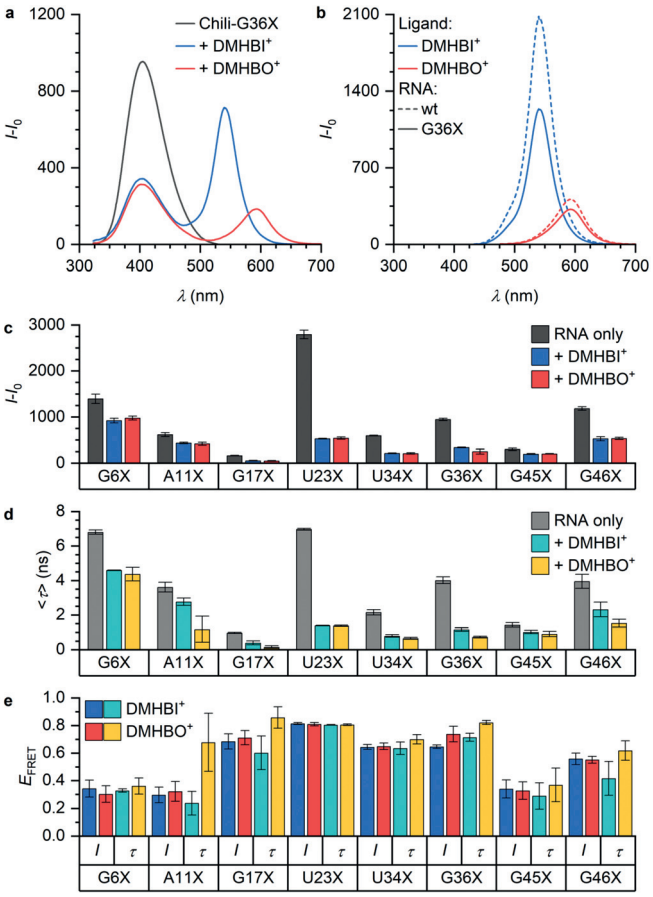

Figure 4. a) Fluorescence emission spectra of Chili-G36X (X = **r4CI**) before and after addition of ligand (0.5 μM RNA, 1.0 μM ligand, 125 mM KCl, 5 mM $MgCl_2$, 40 mM HEPES pH 7.5, $\lambda_{ex}=303$ nm). b) Direct fluorescence emission from the ligand is observed for both unmodified and modified Chili ($\lambda_{ex}=413/456$ nm for $DMHBI^+$/$DMHBO^+$). c) Fluorescence intensity at 410 nm ($\lambda_{ex}=303$ nm) and d) amplitude average fluorescence lifetimes of modified Chili RNAs before and after addition of each ligand. e) FRET efficiencies for **r4CI**-Chili-ligand complexes based on fluorescence intensity and lifetime measurements.

investigated **r4CI**-labeled Chili constructs (Figure 4 and Figure S7). Interestingly, the quantum yield and lifetime of **r4CI** at position G6 (0.48 and 6.8 ns) in the bottom stem region are similar to U23. This may be a result of the absence of immediate guanine neighbors in the sequence but may also indicate that the bottom stem is incompletely formed in the absence of the ligand. This is corroborated by ^{1}H-NMR data of unmodified Chili RNA.[22]

After addition of $DMHBI^+$ or $DMHBO^+$, direct fluorescence of the ligands was observed irrespective of the **r4CI** site, confirming that all modified Chili aptamers were competent to bind and activate emission ($\lambda_{ex/em}=413/542$ nm ($DMHBI^+$) or 456/592 nm ($DMHBO^+$), Figure 4b, Figure S10). Excitation of **r4CI** then resulted in donor-sensitized emission from the bound ligand with a concomitant decrease in donor emission and lifetime (Figure 4c,d and Figures S11 and S12). FRET efficiencies (E_{FRET}) were calculated from the steady-state intensities and amplitude average fluorescence lifetimes

according to the formula $E_{FRET} = 1-(F_{bound}/F_{free})$, with F = fluorescence intensity (I) or lifetime (τ), respectively.[28] The data from both methods (I and τ) were in excellent agreement (Figure 4e) for each RNA–ligand complex. Nearly identical results were obtained with $DMHBI^+$ and $DMHBO^+$ (Table S4), suggesting that both ligands occupy the same binding site in the RNA in comparable orientation.

The calculated values for E_{FRET} contain degenerate information about the donor–acceptor distance (R) and the relative orientation of their transition dipole moments (κ^2).[28] In the case of fluorophores rigidly embedded in a topologically complex system such as the Chili aptamer, and in the absence of additional structure parameters, R and κ^2 are not accessible separately, but need to be evaluated together (Figure 5 and Figure S14). The isotropic Förster radius (R_0)

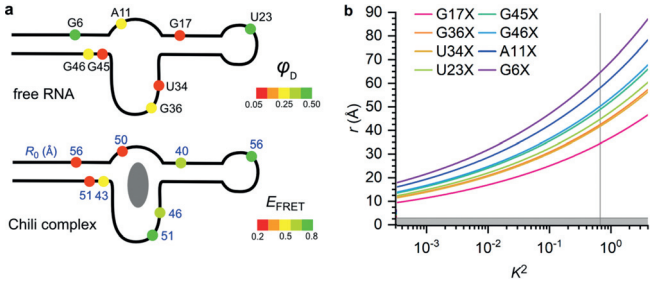

Figure 5. a) Schematic summary of **r4CI** quantum yields at different labeling positions in the free RNA (top) and FRET efficiencies in the ligand bound form (bottom; isotropic R_0 (Å) for $\kappa^2 = 2/3$ given in blue numbers). b) Relationship between the orientation factor κ^2 and possible donor-acceptor (**r4CI**-$DMHBO^+$) distances (r) in eight **r4CI**-labeled Chili aptamers, calculated from measured E_{FRET}, donor quantum yields and overlap integrals (formula in the Supporting Information). The vertical line indicates $\kappa^2 = 2/3$, which would be valid in the dynamic isotropic regime.

assuming $\kappa^2 = 2/3$ is therefore only a superficial guide but cannot be used to derive reliable distance information. Nevertheless, the combined analysis suggests that the bound ligand is coupled more strongly to **r4CI** at G17 than to any other **r4CI** labeled position. Moreover, it suggests U23 as highly suitable **r4CI** labeling position for FRET-based readout of ligand binding, despite its remote location in the apical tetraloop. Chili-U23X may therefore be used for more in-depth analyses of the RNA conformational landscape by variation of solution conditions. Given the accessible dimension of the rather small 52 nt long RNA (shorter than an extended 26mer duplex of ca. 7 nm), the low E_{FRET} of **r4CI** at positions 6, 11, and 46 suggests relative orientations of the transition dipoles that result in κ^2 values significantly smaller than 2/3.

Besides mapping the binding site of the fluorogenic $DMHBI^+$ and $DMHBO^+$ ligands in the Chili aptamer, supramolecular FRET with **r4CI**-labeled RNA also allows insights into binding of non-fluorogenic ligands, such as the neutral precursor of $DMHBI^+$, which carries a dimethylaniline substituent instead of the positively charged side chain (DMHBI-DMA). Significantly reduced **r4CI** emission intensity and lifetime were observed for Chili-U23X upon interaction with the ligand (Figure S13). This result unequivocally confirmed the earlier interpretation[22] that DMHBI-DMA was bound to the RNA, but fluorescence emission was quenched by PET.

In summary, we have developed the synthesis of a ribonucleoside and corresponding phosphoramidite building block containing the fluorescent nucleobase analog 4-cyanoindole. Thermal melting studies revealed that **r4CI** behaves as a truly universal base analog, that is, it is not biased towards any particular hybridization partner among the canonical nucleobases. This property allowed us to incorporate **r4CI** at different sites into the fluorogenic RNA aptamer Chili, where it functions as an ideal intrasupramolecular FRET donor for the non-covalently bound ligands $DMHBI^+$ and $DMHBO^+$, achieving total Stokes shifts between 240 and 290 nm. Steady-state and time-resolved fluorescence of the donor were used to gauge the quantum yield of **r4CI** at each position and obtain the respective energy transfer efficiencies, which depended strongly on the precise incorporation site of **r4CI** and its distance and relative orientation with respect to the bound ligand. The supramolecular FRET efficiencies provided structural restraints of the overall aptamer-ligand organization and identified positions suitable for FRET-based ligand screening. This work represents the first study to use base–ligand FRET with an innately fluorogenic ligand, and it may set the bar for future efforts on less well studied RNA constructs. We anticipate that intrasupramolecular FRET will be a useful tool for supplementing crystallography- and NMR-based structure elucidation methods. Moreover, the FBA–ligand FRET pairs may find applications in nucleic acid nanotechnology, as components of aptamer switches or FRET relay logic gates in molecular sensor devices.

Acknowledgements

This work was supported by the European Research Council (ERC consolidator grant No. 682586). We thank Sebastian Mayer for technical assistance and ESI-MS analyses.

Conflict of interest

The authors declare no conflict of interest.

Keywords: fluorescence resonance energy transfer · isomorphic nucleobase analogues · RNA aptamers · Stokes shift · structure probes

How to cite: *Angew. Chem. Int. Ed.* **2020**, *59*, 6760–6764
Angew. Chem. **2020**, *132*, 6826–6830

[1] a) M. You, S. R. Jaffrey, *Annu. Rev. Biophys.* **2015**, *44*, 187–206; b) E. V. Dolgosheina, P. J. Unrau, *Wiley Interdiscip. Rev. RNA* **2016**, *7*, 843–851; c) R. J. Trachman, A. R. Ferre-D'Amare, *Q. Rev. Biophys.* **2019**, *52*, e8.
[2] J. S. Paige, K. Y. Wu, S. R. Jaffrey, *Science* **2011**, *333*, 642–646.
[3] G. S. Filonov, J. D. Moon, N. Svensen, S. R. Jaffrey, *J. Am. Chem. Soc.* **2014**, *136*, 16299–16308.

[4] K. D. Warner, L. Sjekloca, W. Song, G. S. Filonov, S. R. Jaffrey, A. R. Ferre-D′Amare, *Nat. Chem. Biol.* **2017**, *13*, 1195 – 1201.
[5] C. Steinmetzger, N. Palanisamy, K. R. Gore, C. Höbartner, *Chem. Eur. J.* **2019**, *25*, 1931 – 1935.
[6] E. V. Dolgosheina, S. C. Jeng, S. S. Panchapakesan, R. Cojocaru, P. S. Chen, P. D. Wilson, N. Hawkins, P. A. Wiggins, P. J. Unrau, *ACS Chem. Biol.* **2014**, *9*, 2412 – 2420.
[7] R. Wirth, P. Gao, G. U. Nienhaus, M. Sunbul, A. Jäschke, *J. Am. Chem. Soc.* **2019**, *141*, 7562 – 7571.
[8] S. Neubacher, S. Hennig, *Angew. Chem. Int. Ed.* **2019**, *58*, 1266 – 1279; *Angew. Chem.* **2019**, *131*, 1278 – 1291.
[9] a) S. R. Jaffrey, *Adv. Pharmacol.* **2018**, *82*, 187 – 203; b) R. Wu, A. Karunanayake Mudiyanselage, F. Shafiei, B. Zhao, Y. Bagheri, Q. Yu, K. McAuliffe, K. Ren, M. You, *Angew. Chem. Int. Ed.* **2019**, *58*, 18271 – 18275; *Angew. Chem.* **2019**, *131*, 18439 – 18443; c) M. You, J. L. Litke, R. Wu, S. R. Jaffrey, *Cell Chem. Biol.* **2019**, *26*, 471 – 481.
[10] a) A. Chopra, S. Sagredo, G. Grossi, E. S. Andersen, F. C. Simmel, *Nanomaterials* **2019**, *9*, 507; b) V. Goldsworthy, G. LaForce, S. Abels, E. F. Khisamutdinov, *Nanomaterials* **2018**, *8*, 984.
[11] M. D. E. Jepsen, S. M. Sparvath, T. B. Nielsen, A. H. Langvad, G. Grossi, K. V. Gothelf, E. S. Andersen, *Nat. Commun.* **2018**, *9*, 18.
[12] X. Li, H. Kim, J. Litke, J. Wu, S. Jaffrey, *Angew. Chem. Int. Ed.* **2020**, *59*, 4511 – 4518; *Angew. Chem.* **2020**, *132*, 4541 – 4548.
[13] C. Perez-Gonzalez, D. A. Lafontaine, J. C. Penedo, *Front. Chem.* **2016**, *4*, 33.
[14] a) A. Haller, M. F. Souliere, R. Micura, *Acc. Chem. Res.* **2011**, *44*, 1339 – 1348; b) M. F. Soulière, A. Haller, R. Rieder, R. Micura, *J. Am. Chem. Soc.* **2011**, *133*, 16161 – 16167.
[15] A. Serganov, D. J. Patel, *Annu. Rev. Biophys.* **2012**, *41*, 343 – 370.
[16] W. Xu, K. M. Chan, E. T. Kool, *Nat. Chem.* **2017**, *9*, 1043 – 1055.
[17] A. R. Rovira, A. Fin, Y. Tor, *Chem. Sci.* **2017**, *8*, 2983 – 2993.
[18] M. Bood, S. Sarangamath, M. S. Wranne, M. Grotli, L. M. Wilhelmsson, *Beilstein J. Org. Chem.* **2018**, *14*, 114 – 129.
[19] a) K. Börjesson, S. Preus, A. H. El-Sagheer, T. Brown, B. Albinsson, L. M. Wilhelmsson, *J. Am. Chem. Soc.* **2009**, *131*, 4288 – 4293; b) M. S. Wranne, A. F. Füchtbauer, B. Dumat, M. Bood, A. H. El-Sagheer, T. Brown, H. Graden, M. Grotli, L. M. Wilhelmsson, *J. Am. Chem. Soc.* **2017**, *139*, 9271 – 9280.
[20] a) A. F. Füchtbauer, M. S. Wranne, M. Bood, E. Weis, P. Pfeiffer, J. R. Nilsson, A. Dahlen, M. Grotli, L. M. Wilhelmsson, *Nucleic Acids Res.* **2019**, *47*, 9990 – 9997; b) J. H. Han, S. Yamamoto, S. Park, H. Sugiyama, *Chem. Eur. J.* **2017**, *23*, 7607 – 7613.
[21] Y. Xie, A. V. Dix, Y. Tor, *J. Am. Chem. Soc.* **2009**, *131*, 17605 – 17614.
[22] C. Steinmetzger, I. Bessi, A. K. Lenz, C. Höbartner, *Nucleic Acids Res.* **2019**, *47*, 11538 – 11550.
[23] K. T. Passow, D. A. Harki, *Org. Lett.* **2018**, *20*, 4310 – 4313.
[24] a) J. Božilović, J. W. Bats, J. W. Engels, *Can. J. Chem.* **2007**, *85*, 283 – 292; b) J. J. Chen, Y. Wei, J. C. Drach, L. B. Townsend, *J. Med. Chem.* **2000**, *43*, 2449 – 2456.
[25] Derivation of the curve fitting equation is given in the supporting information.
[26] A. C. Jones, R. K. Neely, *Q. Rev. Biophys.* **2015**, *48*, 244 – 279.
[27] T. Heinlein, J. P. Knemeyer, O. Piestert, M. Sauer, *J. Phys. Chem. B* **2003**, *107*, 7957 – 7964.
[28] *FRET-Förster Resonance Energy Transfer* (Eds.: I. Medintz, N. Hildebrandt), Wiley-VCH, Weinheim, **2014**.

Manuscript received: December 30, 2019
Revised manuscript received: February 11, 2020
Accepted manuscript online: February 12, 2020
Version of record online: March 6, 2020

